Viscoelastic properties of nanocellulose based inks for 3D printing and mechanical properties of CNF / alginate biocomposite gels

Ellinor Heggset[1], Berit L. Strand[2], Kristin W. Sundby[3], Sébastien Simon[4], Gary Chinga-Carrasco[1], Kristin Syverud[1,4*]

[1] RISE PFI, Høgskoleringen 6b, 7491 Trondheim, Norway

[2] NOBIPOL, Department of Biotechnology and Food Sciences, NTNU Norwegian University of Science and Technology, 7491 Trondheim, Norway

[3] Borregaard, Postboks 162, 1701 Sarpsborg, Norway

[4] Department of Chemical Engineering, NTNU Norwegian University of Science and Technology, 7491 Trondheim, Norway

*Corresponding author: kristin.syverud@rise-pfi.no, Tel.: +4795903740

Orcid:

Ellinor Heggset: https://orcid.org/0000-0001-8876-8898

Sébastien Simon: https://orcid.org/0000-0002-3101-4267

Kristin Syverud: https://orcid.org/0000-0003-2271-3637

Gary Chinga-Carrasco: http://orcid.org/0000-0002-6183-2017

Abstract

Inks for 3D printing based on cellulose nanofibrils (CNFs) or mixtures of CNFs and either cellulose nanocrystals (CNCs) or alginate were assessed by determining their viscoelastic properties i.e. complex viscosity and storage and loss moduli (G' and G''). Two types of alginates were used, i.e. from *Laminaria hyperborea* stipe and *Macrocystis pyrifera*. Shape fidelity of 3D printed grids were qualitatively evaluated and compared to the viscoelastic properties of the inks. The biocomposite gels containing alginate were post stabilized by crosslinking with Ca^{2+}. Mechanical properties of the crosslinked biocomposite gels were assessed. The complex viscosity, G' and G'' of CNF suspensions increased when the solid content was increased from 3.5 to 4.0 wt%, but levelled off by further increase in CNF solid content. The complex viscosity at low angular frequency at 4 wt% was as high as 10^4 Pa ·s. This seemed to be the necessary viscosity level for obtaining good shape fidelity of the printed structures for the studied systems. By replacing part of the CNFs with CNCs, the complex viscosity, G' and G'' were reduced and so was also the shape fidelity of the printed grids. The changes in complex viscosity and moduli when CNFs was replaced with alginate depended on the relative amounts of CNFs / alginate. The type of alginate (from either *L. hyp.* stipe or *M. pyr.)* did not play a role for the viscoelastic properties of the inks, nor for the printed grids before post stabilization. Replacing CNFs with up to 1.5 wt% alginate gave satisfactory shape fidelity. The effect of adding alginate and subsequent crosslinking with Ca^{2+}, strongly affected the strength properties of the gels. By appropriate choice of relative amounts of CNFs and alginate and type of alginate, the Young's modulus and rupture strength could be controlled within the range of 30 – 150 kPa and 1.5 – 6 kg, respectively. The deformation at rupture was around 55 %. The alginate from *L. hyp.* stipe yields higher Young's modulus and lower syneresis compared to *M. pyr*. This shows that the choice of alginate plays a significant role for the mechanical properties of the final product, although it does not influence on the viscoelastic properties of the ink. The choice of alginate should be *L. hyp.* stipe if high strength is desired.

Keywords: nanocellulose; alginate; biocomposite; rheology, 3D printing, hydrogels; mechanical properties

Introduction

Nanocellulose is a general term for isolated cellulosic materials, including cellulose nanofibrils (CNFs) and cellulose nanocrystals (CNCs). Depending on the production method, the surface chemistry and morphology of the nanocellulose can be varied, so that tailor-made materials can be produced. Methods for production of CNFs can be e.g. mechanical fibrillation or involve pretreatments; e.g. enzymatic (Pääkkö et al. 2007), TEMPO-mediated oxidation (Saito and Isogai 2004) or carboxymethylation (Wågberg et al. 2008). For CNFs, most of the fibrils have widths in the nanometre scale and lengths in the micrometre scale (Chinga-Carrasco et al. 2014). CNCs, on the other hand, is produced from acid hydrolysis of the cellulose fibre. The fibre consists of both amorphous and crystalline regions, and the acid treatment hydrolyses the amorphous regions, leaving the crystalline parts left. CNC particles are typically ranging from 3 to 5 nm in width and 100 to 200 nm in length (Habibi et al. 2010).

Alginates, which mainly are harvested from brown algae, are linear copolymers of 1→4 linked β-D-mannuronic acid (M) and α-L-guluronic acid (G). The monomers are arranged in a block-wise pattern along the chain forming regions of M- and G-blocks, interspaced with regions of alternating structure (MG-blocks) (Haug et al. 1967).

Hydrogels are three-dimensional polymer / fibril networks with capability to retain a large amount of water. They are often used in biomedical applications as they resemble natural tissue due to the high water content and soft texture. Hydrogels can be composed of biobased or synthetic polymers. They are crosslinked either chemically (by covalent linkages), physically (by hydrogen bonding, hydrophobic interactions and ionic interactions) or by a combination of the two (Peppas and Khare 1993).

Three-dimensional (3D) printing is a technology for the production of objects, layer by layer, through controlled deposition of material (ink). In the medical field, 3D printing is advantageous as customized and personalized products can be produced. However, some challenges with respect to 3D printing of *hydrogels* can be collapsing of the structure and low shape fidelity (Markstedt et al. 2015). Collapsing is usually due to low dry content, while shape fidelity is determined by the viscoelastic properties of the ink. The ink should optimally flow through the nozzle of the printing device and retain the predefined shape during the deposition process. High yield stress is positive for shape fidelity. Nanocelluloses have been applied in several studies (Dai et al. 2019; Huan et al. 2018; Leppiniemi et al. 2017; Rashad et al. 2018; Rees et al. 2015; Siqueira et al. 2017; Wang et al. 2018; Xu et al. 2018), and the shear thinning properties of nanocellulose dispersions are particularly advantageous for 3D printing. Recently, reviews focusing on 3D (bio)printing of CNF-based inks for biomedical applications have been

published (Chinga-Carrasco 2018; Piras et al. 2017; Sultan et al. 2017). Alginate solutions, on the other side, show low viscosity and Newtonian flow, which reduces the shape fidelity and structural stability of printed constructs. Studies have shown that addition of CNFs increase the viscosity and changes the rheological behaviour into shear-thinning (Markstedt et al. 2015; Martínez Ávila et al. 2016; Muller et al. 2017). Crosslinking with divalent cations to (preferentially) the G-blocks, but also the MG-blocks, results in alginate hydrogels with varying mechanical properties (Donati et al. 2005). This applies also for negatively charged qualities of CNFs (Dong et al. 2013; Zander et al. 2014). Several characteristics are important to qualify a material as ink for 3D printing, e.g. printability and mechanical and structural properties. 3D printing that involves inks containing living cells is referred to as 3D *bio*printing and *bio*inks require that the rheological properties should sustain cell viability during the printing process. It is thus most beneficial that the material has shear-thinning properties, which facilitates the extrusion process. Additionally, the thixotropic behaviour of the inks facilitates the ink deposition and consolidation to form free-standing 3D constructs. Nanocellulose-based inks fulfil these requirements.

Hydrogels have been used extensively in many clinical applications, e.g. regeneration of skin, cartilage and bone, as wound dressings and for drug delivery. For these applications, mechanical properties, as well as the biocompatibility and biodegradability are important characteristics. In the recent years, in vitro studies for CNF scaffolds seeded with cells have been reported (Alexandrescu et al. 2013; Markstedt et al. 2015; Martínez Ávila et al. 2016; Muller et al. 2017; Rashad et al. 2017). Good cell adhesion and proliferation, as well as phenotype maintenance have been demonstrated, indicating that the CNF material is non-cytotoxic to the tested cell lines. The water holding capacity and the oxygen permeability, which provides good cellular proliferation and prevents growth of anaerobic bacteria, are also important properties for use in wound healing applications (Poonguzhali et al. 2017). There are differences between CNFs and CNCs, due to their morphological characteristics. Compared to CNFs, CNCs require higher concentrations to achieve percolation. Increased concentration may again affect the stiffness of the scaffold, which is an important factor in e.g. tissue engineering applications (Syverud 2017). The elasticity (stiffness) of scaffolds influences the development of stem cells into differentiated cell types (Engler et al. 2006). The choice of materials and, if possible, the tuning of their mechanical properties, should be based on the prerequisite of the final mechanical properties of the printed product. Aarstad and colleagues have shown that biocomposite gels of CNFs and alginate revealed properties like high rupture strength, high compressibility, high gel rigidity at small deformations (Young's modulus) and low syneresis

(Aarstad et al. 2017). The effects varied with relative amounts of CNFs and alginate, the source of alginate and the CNF quality. Hence, by combining the two biopolymers in biocomposite gels, it was possible to tune rupture strength, Young's modulus and syneresis.

A challenge with hydrogels is that they in general are weak (De France et al. 2017). The mechanical properties are sufficiently strong for soft tissue like skin or muscles, but remain too weak for load bearing structures like cartilage and bone in which mechanical stability is essential. One way to increase the strength is to increase the solid content of the hydrogels as the mechanical properties are strongly dependent on this (e.g. (Aarstad et al. 2017)). However, all rheological properties are also heavily dependent on the solid content in the suspension (i.e. ink), with power law dependency of storage modulus and viscosity (e.g. (Naderi et al. 2014)). In 3D printing, the flow properties of the ink are essential meaning that the solid content of the suspension cannot be increased to a level in which the injection force is too high to extrude the ink. In the present work we study viscoelastic properties and printability of CNF inks and biocomposite inks of CNFs and either CNCs or alginate. For the biocomposite inks we explore the rheological properties at constant and relatively high solid content, and how they are influenced by the relative amounts of the components. The solid content is increased compared to a previous study on *cast* CNF-alginate composite gels (from 1.75 wt % (Aarstad et al. 2017) to 4.5 wt %). The aim is to obtain inks that give *3D printed* hydrogels with higher strength by using higher solid content. Furthermore, the mechanical properties of Ca^{+} crosslinked CNF / alginate biocomposite gels were assessed.

Materials and methods

Materials

Nanocellulose

Cellulose nanofibrils (CNFs)

The CNFs were an Exilva Forte grade, produced at Borregaard's production facility in Sarpsborg, Norway, and uses Norwegian spruce as the raw material. Exilva is provided as a gel with a solid content of 10 wt.%.

Cellulose nanocrystals

The cellulose nanocrystals (CNCs) were manufactured at the Forest Products Laboratory in Madison, USDA (U.S. Dep. Of Agriculture). The material was produced using 64 % sulphuric acid to hydrolyse the amorphous regions of the cellulose material, resulting in acid resistant

crystals with some surface sulphate groups. The sulphate charge density was 0.3 mmol/g (Heggset et al. 2017). The stock dispersion has a concentration of 12.2 wt.%.

Alginate

Alginate from *Laminaria hyperborea* stipe was obtained from DuPont (previous FMC Health and Nutrition, Sandvika, Norway), and alginate from *Macrocystis pyrifera* was purchased from Sigma-Aldrich (St. Louis, Missouri, USA). Molecular weight and composition given as fractions of monomers, dimers and tetramers as well as an estimate of G-block length is given in Table 1.

Table 1. Molecular weight (M_w) and sequence parameters of alginates used in this study[1].

Alginate source	M_w (kDa)	PI	F_G	F_M	F_{GG}	F_{GM}	F_{MM}	F_{MGM}	F_{GGG}	$N_{G>1}$
M. pyrifera	177	1.94	0.41	0.59	0.21	0.20	0.40	0.18	0.17	5
L. hyperborea	126	1.86	0.66	0.34	0.55	0.11	0.23	0.08	0.51	14

[1] M_w and polydispersity index (PI = M_w/M_n) were determined from SEC-MALLS. Sequence parameters were calculated from ^{1}H-NMR spectra. F_G and F_M denote the fraction of guluronic and mannuronic acid, respectively. Fractions of dimers and trimers of varying composition are denoted by two and three letters, respectively. $N_{G>1}$ is the average G-block length.

Characterization of CNFs.

Atomic Force Microscopy.

The microscopic features of the composite samples were studied by atomic force microscopy (AFM), using a Bruker Multimode V AFM equipped with a Nanoscope V Controller (Veeco Instruments Inc., Santa Barbara, CA, USA). The instrument was located at the NorFab facility NTNU Nanolab in Trondheim.

A drop of the dispersion (0.1 wt%) was placed on freshly cleaved 10 mm mica (Agar Scientific Ltd., Essex, UK), and dried using compressed nitrogen gas (N_2) before the image could be taken. Images were obtained by ScanAsyst mode in air at ambient conditions. The ScanAsyst-Air AFM tips were provided by Bruker AFM Probes (Bruker Nano Inc., Camarillo, CA, USA).

Determination of surface groups.

The content of carboxyl and aldehyde groups was determined by conductometric titration, as described by Saito and colleagues (Saito and Isogai 2004). The equipment used was a 902 Titrando with a Metrohm 856 Conductivity Module, and the data was recorded by Tiamo Titration Software. The carboxylate content was calculated from the titration curve obtained. This analysis was also done after oxidation of aldehyde groups to carboxyl groups using $NaClO_2$. The difference in carboxylate content before and after the $NaClO_2$ oxidation yields the aldehyde content (Saito and Isogai 2006).

Preparation of samples.

The Exilva stock solution was diluted to 3.5, 4.0 and 4.5 wt%, respectively. Additionally, composite samples of Exilva and additive (CNCs, alginate) were prepared as described in Table 2. The mixtures were added a freshly made solution of 30 mM D-glucono-lactone (GDL), to prepare the gels for crosslinking (after 3D printing). The final dry content of all the composite samples was 4.5 wt%.

Table 2. Sample overview. Identification of samples prepared in the study, the forming methods and methods used for analyses. The total solid content was 4.5 wt% for all the composite samples.

Sample no.	Exilva, solid content (%)	Additive	Solid content of additive (%)	Total solid content (%)	Forming method	Analyses
1	3.5	-		3.5	3D printing	Rheology
2	4.0	-		4.0	3D printing	Rheology
3	4.5	-		4.5	3D printing	Rheology
4	4.0	CNCs	0.5	4.5	3D printing	Rheology
5	3.5	CNCs	1.0	4.5	3D printing	Rheology
6	3.0	CNCs	1.5	4.5	3D printing	Rheology
7	4.0	*L. hyp.*	0.5	4.5	3D printing Casting	Rheology Texture analyser
8	3.5	*L. hyp.*	1.0	4.5	3D printing Casting	Rheology Texture analyser
9	3.0	*L. hyp.*	1.5	4.5	3D printing Casting	Rheology Texture analyser
10	4.0	*M. pyr.*	0.5	4.5	3D printing Casting	Rheology Texture analyser
11	3.5	*M. pyr.*	1.0	4.5	3D printing Casting	Rheology Texture analyser
12	3.0	*M. pyr.*	1.5	4.5	3D printing Casting	Rheology Texture analyser

Rheology assessment of inks for 3D printing.

The rheological properties of samples were determined using a Physica MCR 301 rheometer (Anton Paar GmbH, Graz, Austria) equipped with a plate-plate geometry (diameter = 5 cm) at a gap size of 1 mm. The top and bottom surfaces are cross-hatched to reduce wall slip effect. The samples were loaded onto the bottom plate and the top plate was lowered at the right position. The sample was allowed to rest for 15 minutes. Then, oscillatory measurements were performed: first a frequency sweep between 100 and 0.1 Hz at a strain of 0.5% to obtain the structure of the interfacial film, and secondly a strain sweep between 0.01 and 100% at a frequency of 1 Hz to determine the linear viscoelastic range. Two parallels were performed for each sample at a temperature of 20 °C.

3D printing of hydrogels.

3D printing was performed with the Regemat3D printing unit (version 1.0). Grids of 20 mm diameter and 2 mm height (4 layers) were designed with the Regemat3D Designer (version 1.8, Regemat3D, Granada, Spain) and printed by micro-extrusion (direct ink writing). The structures were printed with a conical nozzle (size 0.58 mm) and the flow speed during printing was 3.0 mm/s. Four grids were printed for each series. Afterwards, the CNF / alginate 3D printed structures were soaked in a solution containing 50 mM Ca^{2+} ions for post stabilization. The post-crosslinking process was performed for at least 48 hours at room temperature.

Casting of gel cylinders.

In order to assess the mechanical properties of post stabilized CNF / alginate biocomposite gels, samples suitable for testing in the texture analyser instrument were prepared, i.e. cast gel cylinders. Biocomposite gels with alginate and Exilva were made by mixing alginate powder with MQ water and subsequently adding the Exilva dispersion. The suspensions were dissolved under heavily stirring. Gel cylinders were prepared by internal gelling with $CaCO_3$ and GDL as previously described by Aarstad and colleagues (Aarstad et al. 2017). 15 mM $CaCO_3$ (particle size 4 µm) was added to the alginate / Exilva solution. The concentrations of Exilva / alginate were as given in Table 2. Further, the mixture was added a freshly made solution of 30 mM GDL. The total volume of the suspensions was 100 mL of each blend. The mixture was immediately poured onto a petri dish and gel cylinders were stamped out from the mixture. The cylinders were left at room temperature for minimum 20 h for complete gelation, and the moulds were under pressure during incubation. Subsequently, the gel cylinders were removed from the moulds before being immersed in a solution of 50 mM $CaCl_2$ and 200 mM NaCl and left for at least 24 h at 4 °C for calcium saturation before compression measurements at the texture analyser.

Texture analysis of cast gels.

Force/deformation curves was recorded at 22 °C on a Stable Micro Systems TA-XT2 texture analyser equipped with a P/35 probe and at a compression rate of 0.1 mm/s (Mørch et al. 2008). A number of 6-8 gels were measured per sample. The gels were subjected to uniaxial compression surpassing the point of rupture, where force and deformation was recorded. Young's modulus was calculated as G*(h/A) where G is the initial slope (N/m) of the stress deformation curve and h and A is the height and area of the gel cylinder, respectively.

Results and Discussion

Nanocellulose characteristics

Charge density of the Exilva CNFs were determined by conductometric titration to be 106 µmol/g carboxylic acids and 256 µmol/g aldehyde groups. For the CNC quality, the sulphate charge density was approx. 300 µmol/g, as determined by inductively coupled plasma – atomic absorption (ICP-AA) (Heggset et al. 2017).

AFM images of the nanocellulose samples are shown in Figure 1. The Exilva CNF (Fig 1 – top) possess a tight entanglement network of fibrils with varying fibril diameters. The CNC particles show a more brick-like morphology (Fig 1 – bottom), in accordance with what is reported in literature (e.g. (Habibi et al. 2010)).

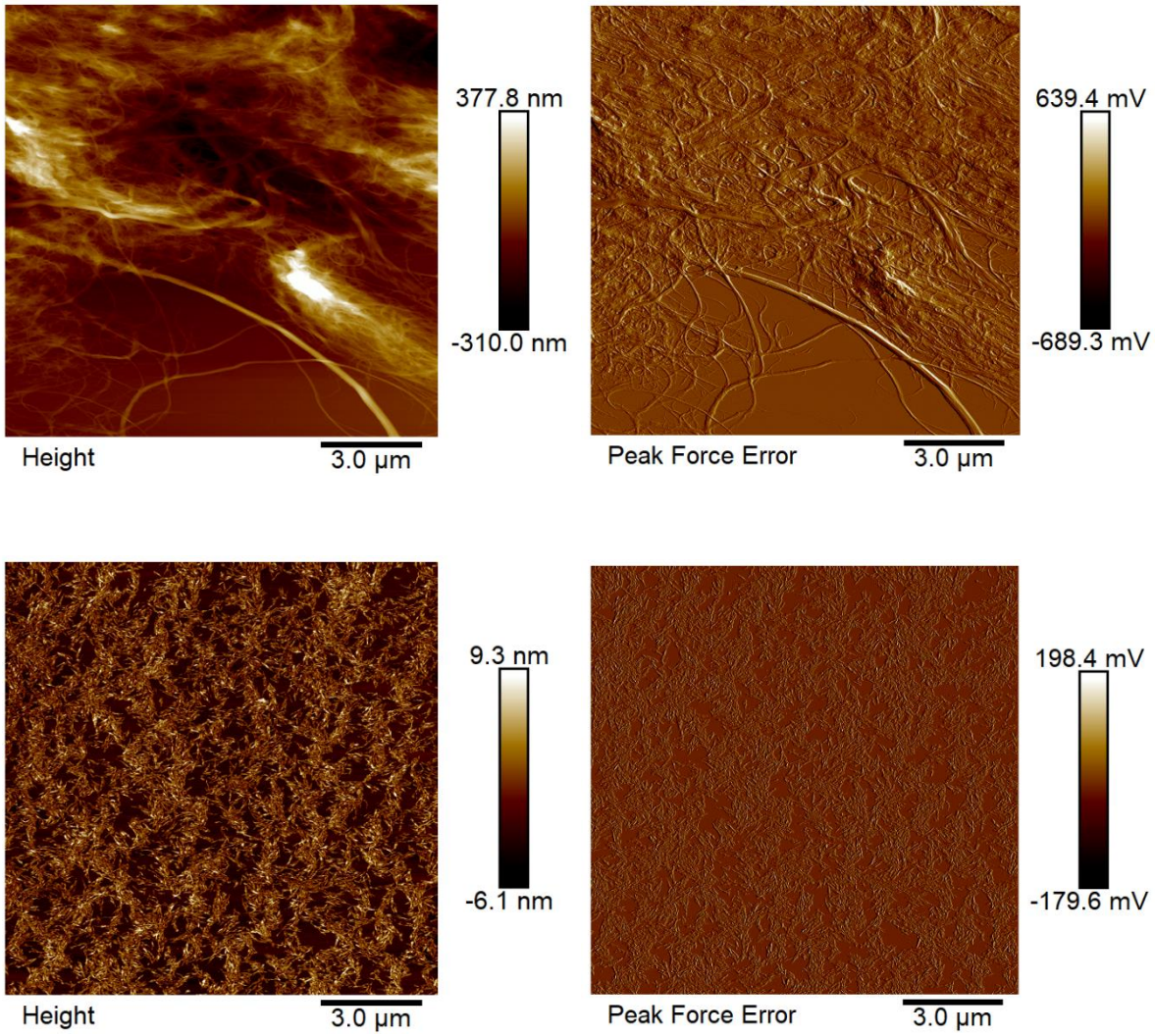

Figure 1. AFM images of the Exilva (top) and CNC (bottom) qualities used in the biocomposite gels.

Rheological properties of CNFs and the composite systems.

As mentioned in the introduction section, the rheological properties of inks are important for 3D printing application. The ink should display shear-thinning behavior to facilitate extrusion as well as high viscosity at rest (i.e. zero or low shear rates) to retain its shape after the printing process. It is therefore important to characterize the flow behavior i.e. the curve viscosity as a function of shear rate for potential 3D printing application. Attempts was done to determine flow curves of investigated systems using a plate-plate geometry with cross-hatched surfaces to prevent wall slip. These attempts were proved unsuccessful because the samples formed lumps during the measurements. Consequently, it was decided to perform oscillation tests to study the rheological properties of CNF mixtures. These oscillation test consisted first of a rest period, followed by a frequency sweep to study the internal structure of samples and finally a strain sweep to determine the linear viscoelastic range.

Figure 2 presents the results of frequency sweeps i.e. variations of G’ and G’’ as a function of oscillation frequency for samples containing only CNFs, and at different CNF concentrations. These variations are similar for the three samples investigated with a higher value of G’ compared with G’’, no crossover point, and a constant to slight increase of G’ and G’’ with frequency. These behaviors are typical of mostly elastic character samples.

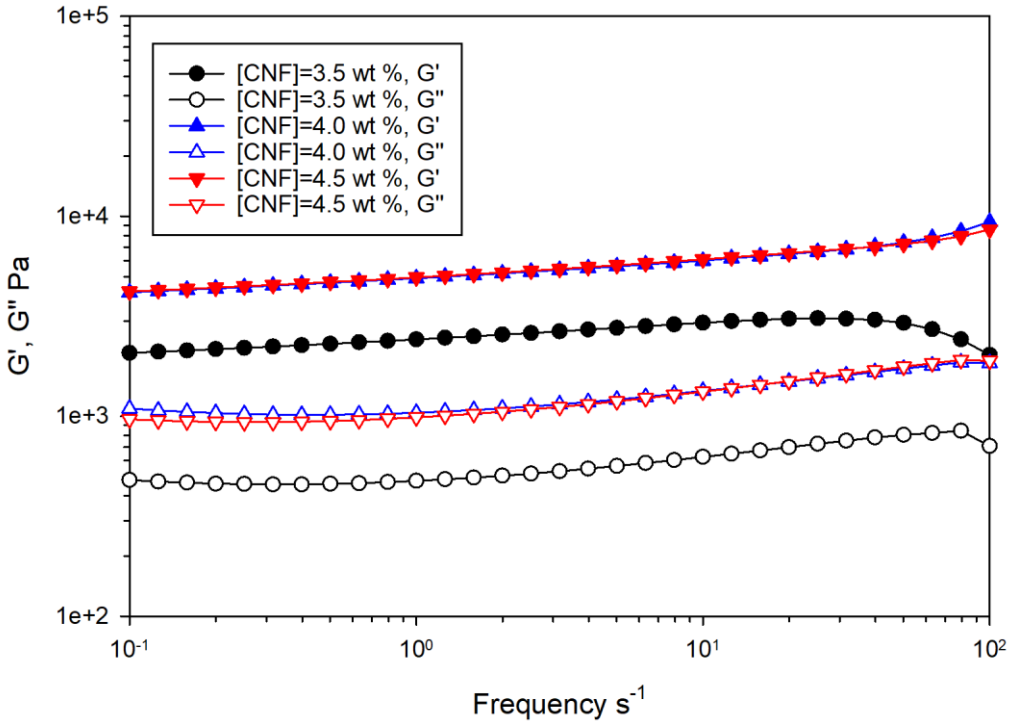

Figure 2. Frequency sweeps for samples containing only CNFs i.e. samples 1, 2, and 3 in Table 2. The CNF content varies from 3.5 wt % for sample 1 to 4.5 wt % for sample 3. Strain = 0.5%.

As previously mentioned, we are mostly interested in the flow curves of the CNFs and CNCs or alginate mixtures for 3D printing applications. Consequently, we have applied the Cox-Merz rule (Al-Hadithi et al. 1992; Cox and Merz 1958) to deduce flow curves from oscillatory frequency sweeps. The Cox-Merz rule, initially observed in 1958, states the correspondence between the steady state shear viscosity plotted as a function of shear rate with the complex viscosity, $|\eta^*|$, plotted as a function of the angular frequency, ω. This rule was observed to apply for many polymeric systems even if some deviations have been observed for some specific systems. We have, therefore, used this rule to study the flow behavior of CNFs and their mixtures. Figure 3 presents the flow curves for the different systems investigated to determine the influence of concentration of CNFs (Figure 3a), CNCs (Figure 3b), alginate from *L. hyp.* (Figure 3c), and alginate from *M. pyr.* (Figure 3d).

The flow curve for all the systems present similar features: No plateau is visible at low and high angular frequency corresponding to low and high shear rates and a pronounced shear thinning behavior is seen over a large angular frequency range (from 0.63 to 630 s^{-1}). The shear thinning index, n, defined by the following relation (Eq. 1) varies from 0.07 to 0.15 as a function of the system.

$$\eta^* = k \cdot \omega^{n-1} \quad \text{(Eq. 1)}$$

This behavior is attributed to the alignment of fibers under shearing. The complex viscosity measured at the lowest applied angular frequency is high. This viscosity depends on the system but is in the order of 10^4 Pa·s.

The viscosity is influenced by the exact composition of the systems. All of the nanocellulose based inks had shear thinning properties. Figure 3a presents the influence of CNF concentration. The complex viscosity increases with CNF concentration when the concentration is increased from 3.5 to 4.0 wt%, then it is more or less constant. The Figures 3b to 3d show the influence of replacing part of the CNFs and mixing with other thickeners (CNCs and two types of alginates). The total concentration of CNFs and the other thickeners was kept constant at 4.5 wt%. Replacing CNFs by increasing concentrations of CNCs resulted in a decrease in complex viscosity (Figure 3b). CNC particles are significantly shorter than CNFs which results in lower viscosifying properties. The two types of alginates present very similar properties when mixed with CNFs (Figure 3c and 3d.). The variations in complex viscosity with alginate concentration in the mixtures with CNFs are relatively small, smaller than for CNCs. However, it seems that the complex viscosity increases when small amount of alginate is added (0.5 wt%), and then decreases at higher alginate concentration. The change in complex viscosity by replacing 0.5 wt% CNFs with either CNCs or alginate caused very small changes. This is in accordance with the fact that the complex viscosity was not increased by increasing the solid content of CNFs from 4.0. to 4.5 wt% in the pure CNF samples. It seems that the complex viscosity is strongly influenced by the solid content of CNFs up to 4 wt%, but then levels off. Above the critical overlap concentration which is about 0.2 to 0.3 wt% CNFs (depending of the degree of fibrillation and length of the fibrils), a network begins to form due to entanglement of fibrils (Lowys et al. 2001). Power law relationship has been assessed for shear viscosity of carboxymethylated CNFs for a solid content range of CNFs from 0.3 to 2.6 wt% (Naderi et al. 2014). A strong increase in viscosity with increased solid content has also been reported for low charged CNFs more similar to the CNFs used in the current study from sugar-beet pulp (0.25 to 3 wt%) (Agoda-Tandjawa et al. 2010) and bleached sulphite pulp (0.25 to 5.9 wt%) (Pääkkö et al. 2007).

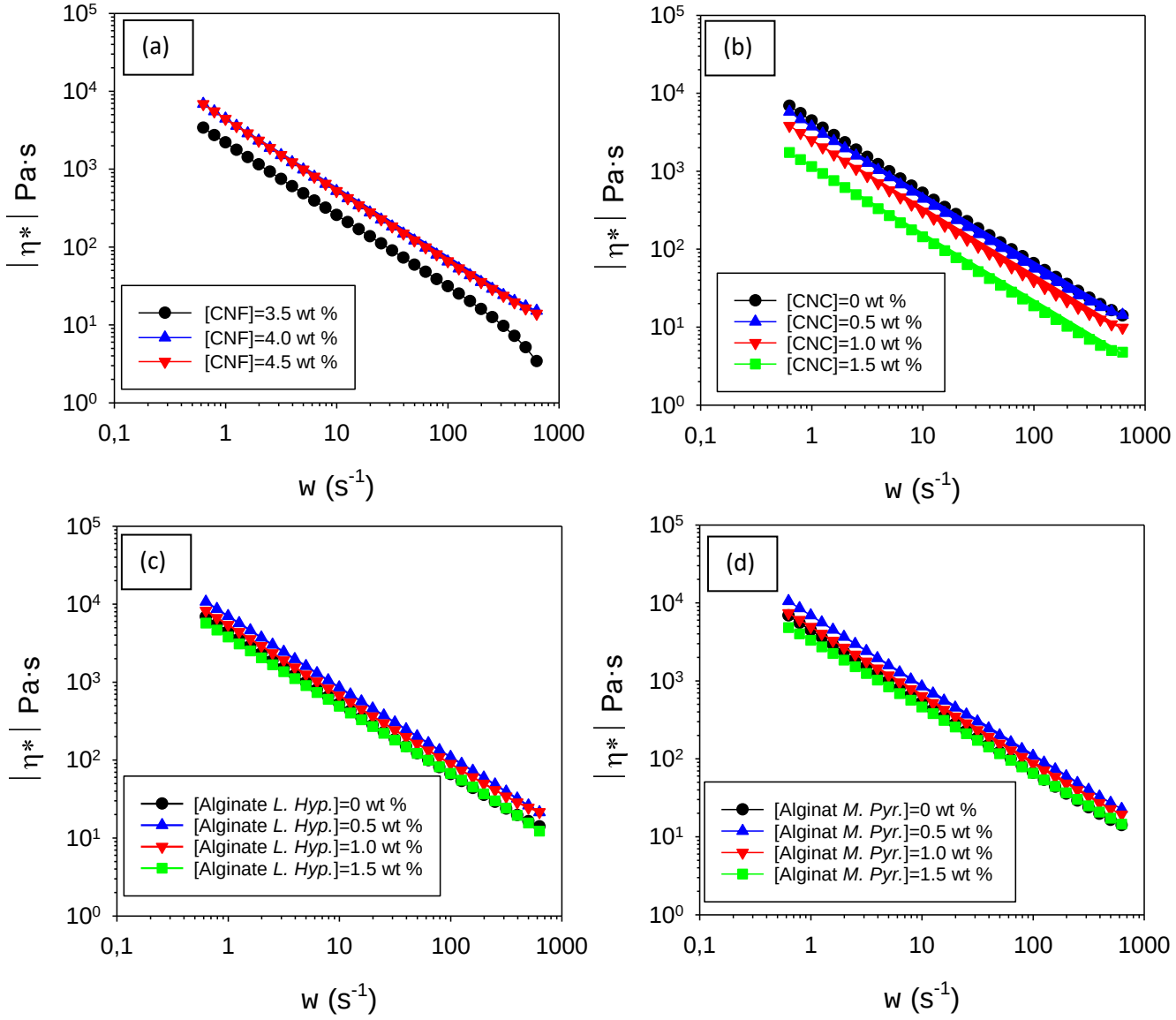

Figure 3. Flow curves, complex viscosity as a function of angular frequency, determined from frequency sweep (strain = 0.5 %) for a) samples containing only CNFs (numbers 1, 2, and 3), b) CNFs and CNCs (numbers 3, 4, 5, and 6), c) CNFs and alginate from *L. hyp.* (numbers 3, 7, 8, and 9), and d) CNFs and alginate from *M. pyr.* (numbers 3, 10, 11, and 12). The total concentration of CNFs + CNCs or alginate in all the systems in Figure b, c, and d is equal to 4.5 wt %.

Strain sweeps were finally performed to determine the critical strain characterizing the transition between linear and non-linear viscoelastic range. Figure 4 presents the strain sweeps obtained for mixtures of CNFs and CNCs (systems numbers 3, 4, 5, and 6). They are

representatives for the other investigated systems. The curves are typical of viscoelastic systems with G' higher than G'' in the linear viscoelastic range. The critical strain, taken as the strain at which G' has decreased by more than 5 % compared with its plateau value, is comprised between 0.16 and 0.4 % for all the samples measured.

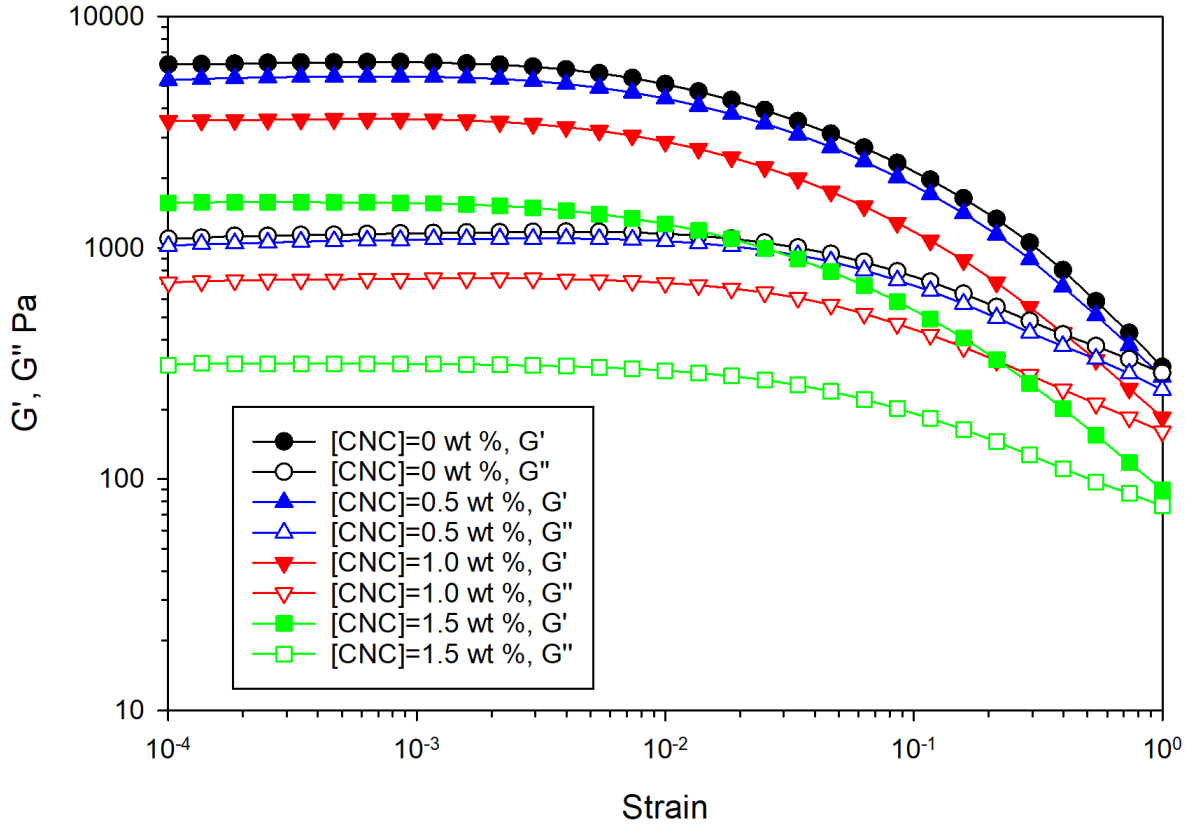

Figure 4: Strain sweeps for samples containing CNFs and CNCs i.e. samples number 3 (no CNCs), 4, 5, and 6. The total concentration of CNFs + CNCs is equal to 4.5 wt %. Frequency = 1 Hz.

3D printing

Figure 5 and 6 show the 3D printed grids of the samples summarized in Table 2. Pictures are taken before crosslinking in Ca^{2+} solution, showing that the shape fidelity is more or less maintained after 3D printing, retaining the designed structure of the grids. Minor differences can be observed between the samples. Figure 5 shows pure CNF samples varying in solid content from 3.5 to 4.5 wt%. The sample with the lowest solid content seems to lose integrity. In row 1 of Figure 6, parts of the CNFs are replaced with CNCs, with increasing amounts of

CNCs from left to right. There is a visible loss in shape fidelity as the CNF content is reduced. This is not the case when CNFs are replaced with alginate (Figure 6, row 2 and 3). These samples show denser structure without loss in shape fidelity. This can be due to changed rheological properties for the composite samples of CNFs and alginate. A complex viscosity of about 10^4 Pa·s at low angular frequency seems to be required for maintaining shape fidelity of these samples. This is obtained in pure CNF samples of 4 wt% solid content, and for the composite inks of CNFs and alginate.

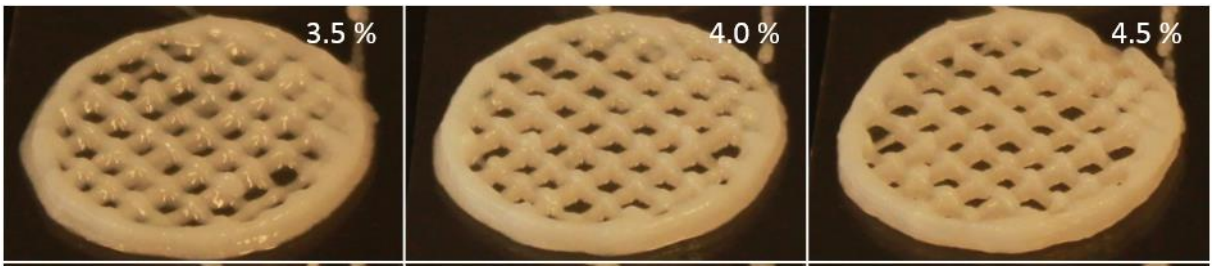

Figure 5. 3D printed grids of the pure Exilva CNF quality. Total dry content is 3.5, 4.0 and 4.5 wt%, respectively.

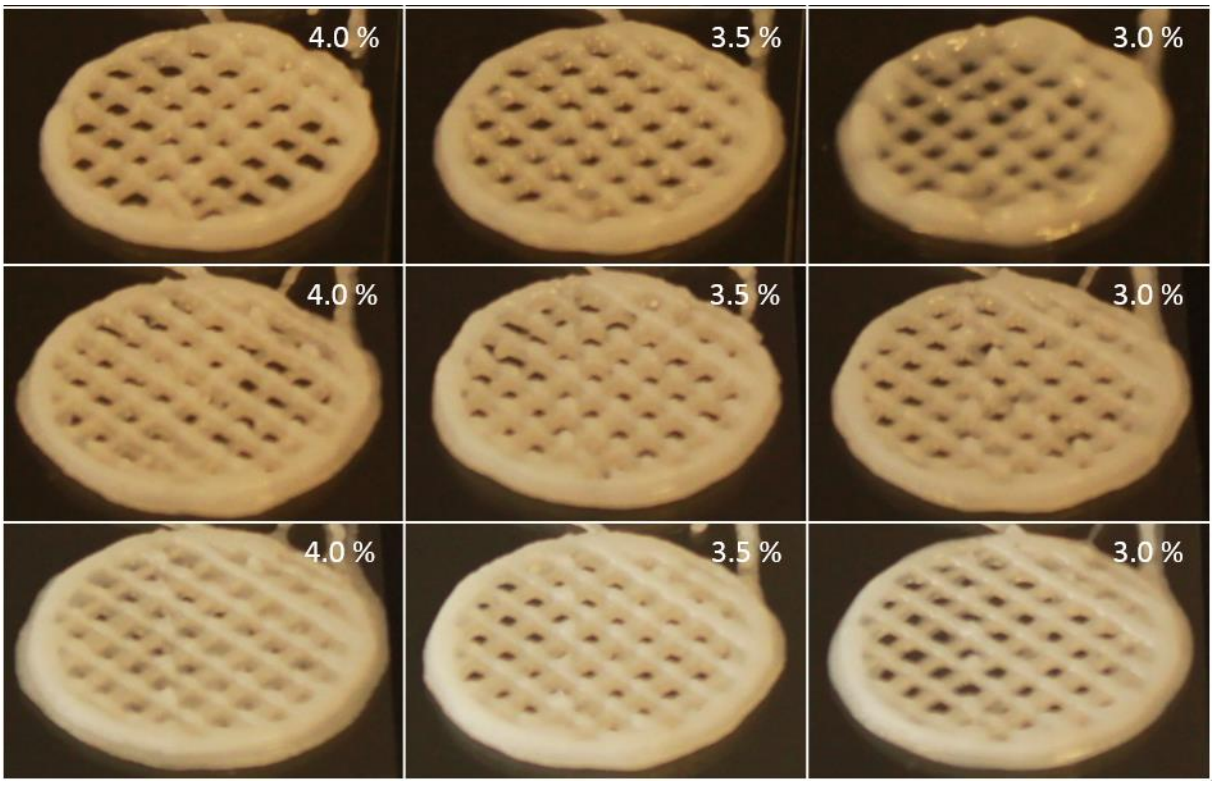

Figure 6. 3D printed grids of the biocomposite samples summarized in Table 2. Row 1 (from top): Exilva with CNCs. Row 2: Exilva with alginate from *L. hyp.*. Row 3: Exilva with alginate from *M. pyr.*. The total dry content is 4.5 wt % in all samples. The dry content of the CNF part is shown for each grid in the Figure.

3D printed structures of nanocellulose can lose their integrity when mechanical stress is applied. This is particularly a limitation at low concentrations of the material (Chinga-Carrasco 2018). Stabilization of the nanocellulose structures is therefore advantageous (De France et al. 2017). In our study, a post stabilization was performed, soaking the 3D printed grids in a solution of Ca^{2+} ions, thus crosslinking and increasing the mechanical properties of CNF /alginate systems (Aarstad et al. 2017). Figure 7 shows a 3D printed structure after post stabilization. The structure holds good viscoelastic properties and did not collapse after mechanical handling.

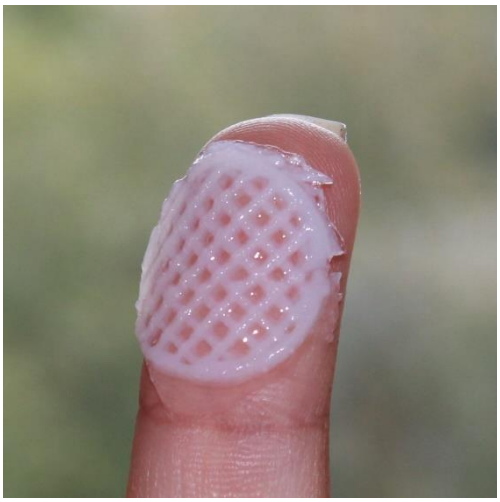

Figure 7. Example of a 3D printed grid containing CNFs and alginate (3.0 wt%: 1.5 wt%; sample 9 in Table 2). The picture is taken after post stabilization of the structure in Ca^{2+} solution.

Mechanical properties of the composite hydrogels of CNFs and alginate

The biocomposite hydrogels of Exilva CNFs and alginate (from *L. hyp.* and *M. pyr.*) saturated with calcium (Figure 8) were measured with respect to gel rigidity (Young's modulus), syneresis (i.e. volume reduction upon gel formation), resistance to breakage and deformation at breakage (Figure 9). The biocomposite gels with alginate from *L. hyp.* showed higher Young's modulus, and reduced syneresis, compared to the gels with alginate from *M. pyr.* This is in accordance with our previous work on CNF / alginate composite hydrogels (Aarstad et al. 2017).

The increase in Young's modulus were correlated with an increased amount of *L. hyp.* alginate. Alginates with high G-content, as alginate from *L. hyp.*, is known to form strong gels after crosslinking with calcium ions (Smidsrod 1972). The same trend was observed for the syneresis: A decrease in syneresis was observed when an increased amount of *L. hyp.* alginate was added. For the biocomposite gels with CNFs and alginate from *M. pyr.*, the Young's modulus was nearly not affected by the increased addition of alginate. For the syneresis, a slightly lower shrinkage was observed for the gels with the lowest alginate addition (CNFs/alg: 4/0.5), compared to the other two biocomposite gel systems, which shows equal syneresis.

We have previously shown that Ca-gels of CNFs alone (0.75 %) does not display syneresis (Aarstad et al. 2017). Hence, the syneresis in composite gels of alginate and CNFs can be

attributed to the content of alginate in the hydrogel. Syneresis of alginate gels is known to be correlated to the content of G-blocks (Donati et al. 2005) as long G-blocks leads to an extended network and less syneresis. This has in particular been shown when adding long G-blocks to alginate gels that resulted in decreased syneresis (Aarstad et al. 2013). On the other hand, MG-blocks are shown to be crosslinked by Ca^{2+}, and alginates containing high amounts of MG are highly syneretic (Donati et al. 2005; Mørch et al. 2007). This can explain the difference in syneresis observed for the two types of alginates used as they vary with regard to both G-blocks and MG-blocks with alginate from *L. hyp.* stipe containing typically a high amount of long G-blocks and alginate from *M. pyr*. having a high content of MG (fraction of F_{GGG} and F_{MGM}, see Table 1 (Aarstad et al. 2012)). We have previously shown that the syneresis of alginate gels is dependent on the concentration of alginate with increased syneresis at lower concentrations for gels with alginate from *M. pyr.* (Aarstad et al. 2017). Here, a reduction in syneresis with increasing concentrations of alginate could be seen for the alginate from *L. hyp.* stipe. The opposite was the case for alginate from *M. pyr*. where an increase in syneresis for increasing concentrations of alginate was seen. This was opposite to our previous observations (Aarstad et al. 2017). However, the concentration range of both alginate and CNFs was different in the two systems and may explain the apparent discrepancy in the results.

The rupture strength of the hydrogels was increasing when an increased amount of alginate was added to the gels. The values were equal for the two different systems, except for the CNFs / *M. pyr.*: 3/1.5 where an increase in the rupture strength compared to CNFs / *L. hyp*.: 3/1.5 was observed (Figure 9). In our previous study, no significant effect of the presence of fibrils was seen on the rupture strength of the alginate gels, except for an increase in the rupture strength for gels of *M. pyr.* alginate when adding mechanically fibrillated CNFs. The rupture strength for these hydrogels were around 5.0-5.5 kg (Aarstad et al. 2017). As previously discussed, alginate gels with a high G-content form strong gels, due to their crosslinking possibilities in the G-blocks. This is observed in the Young's modulus results for the *L. hyp.* alginate. The alginate from *M. pyr.* show large flexibility due to a high content of MG-blocks and can therefore withstand substantial deformations. The deformation at rupture was nearly identical within the two different composite systems, and they did not show a large variation between the two systems. The values were around 55 % deformation at rupture. This means that the CNF / alginate biocomposite gels have good ability to be deformed by either stretching or compressing without breaking. This is considered to be important for many applications, e.g.

for wound dressings, because certain tensile strength, flexibility and elastic properties are needed for handling and replacement (Unnithan et al. 2014).

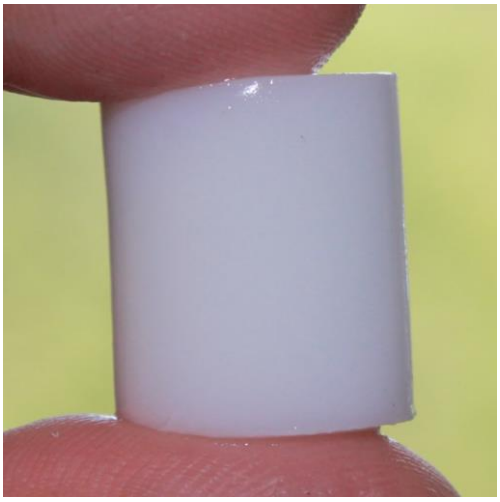

Figure 8: Example of a cast hydrogel containing CNFs and *L. hyp.* alginate (3.0 wt%: 1.5 wt%; sample 9 in Table 2).

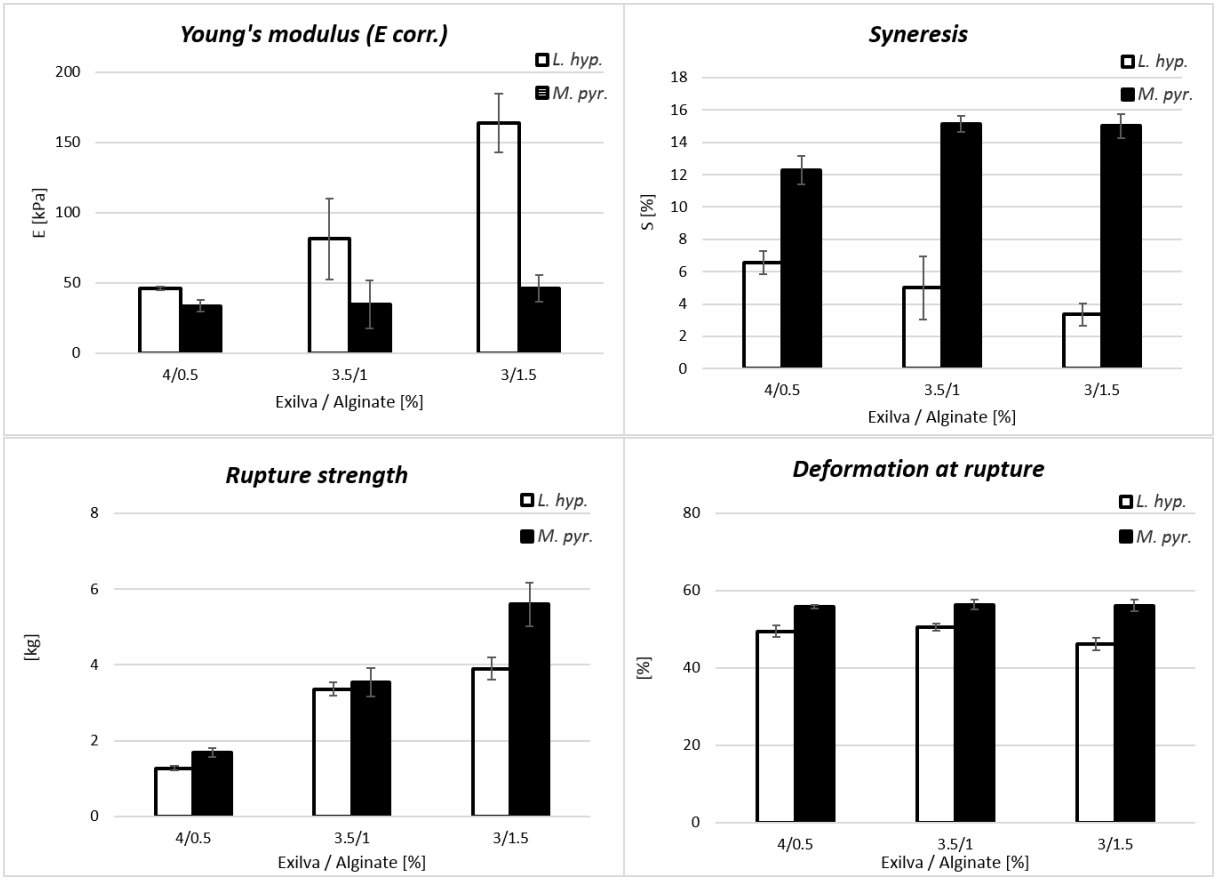

Figure 9: Young's modulus (E), syneresis, rupture strength measured as the force at rupture and compression at rupture of CNF/alginate composite Ca-gels. Bars are ± standard deviations, shown for n = 6-8 gels.

Hydrogels for use in tissue engineering in load bearing structures (cartilage, bone) will need mechanical properties much higher than obtained in the present study. For example, hydrogels for replacement of articular cartilage require Young's modulus of around 1 MPa, high toughness (1000 J/m2) and a water content of 60-80%. However, conventional hydrogels obtained from e.g. chemical reactions have low stiffness (< 10 kPa), low tensile strength (<100 kPa) and low toughness (<100 J/m2) (Nascimento et al. 2018). The CNF / alginate biocomposite gels prepared in the current study have Young's modulus of from 30 - 170 kPa. The uppermost values are relatively high to be physical gels. The solid content of a hydrogel plays a major role in the mechanical properties, provided that there is physical entanglements and network structure between the particles, and / or chemical interactions (hydrogen bonds, ionic or covalent bonds). The current study has shown that when some CNFs are replaced with CNCs, the complex viscosity is reduced. This opens up for the possibility to increase the total solid content in the ink for 3D printing without exceeding a threshold where the injection force necessary to extrude the ink will be too high. A post stabilization is however also necessary for obtaining a stable gel with improved mechanical properties. This can be obtained by several methods, i.e. by mixing the three components CNFs, CNCs and alginate and stabilize with Ca^{2+} crosslinking.

Conclusions

The viscoelastic properties of nanocellulose based inks were strongly influenced by their solid content and by their composition when the solid content was kept constant. The complex viscosity at low angular frequency was as high as 10^4 Pa ·s. By replacing part of the CNFs with CNCs, the complex viscosity and storage and loss moduli were reduced, while the changes in complex viscosity and moduli when CNFs was replaced with alginate depended on the relative amounts of CNFs / alginate. The type of alginate (either from *L. hyp.* or *M. pyr.)* did not play a role for the viscoelastic properties of the inks. It was possible to 3D print the studied CNF quality and get sufficient shape fidelity of the printed structures provided that the CNF solid content was approximately 4 wt%. Shape fidelity of the printed structures was gradually lost

by replacement of CNFs with increasing amounts of CNCs. Replacing CNFs with up to 1.5 wt% alginate gave satisfactory shape fidelity. By appropriate choice of relative amounts of CNFs and alginate and type of alginate, the Young's modulus and rupture strength can be controlled within the range of 30 – 170 kPa and 1.5 – 6 kg, respectively, with a deformation of around 55 % at rupture. This range can most probably be increased by adding CNCs to the CNF / alginate inks to increase the total solid content of the composite. CNCs reduced complex viscosity and will not cause an increase in viscosity that obstruct printing. After crosslinking with Ca^{+}, the alginate from *L. hyp.* stipe gave higher Young's modulus and lower syneresis compared to alginate from *M. pyr*. This shows that the choice of alginate play a significant role for the mechanical properties of the final product, although it does not affect the viscoelastic properties of the ink. The choice of alginate should be *L. hyp.* if high strength is desired. The obtained biocomposite gels have properties suitable for e.g. wound dressings and face masks.

Acknowledgements

This work has been funded by the Research Council of Norway through the NORCEL project, (Grant no. 228147). The AFM images were acquired using instruments available at NTNU NanoLab/NorFab. The Research Council of Norway is acknowledged for the support to the Norwegian Micro-and Nano-Fabrication Facility, NorFab, project number 245963/F50. We would like to thank Ingebjørg Leirset, Birgitte H. McDonagh, Ina S. Pedersen, Wenche I. Strand and Anne Marie Falkenberg Olsen for their technical support during this work.

References

Aarstad O, Heggset EB, Pedersen IS, Bjørnøy SH, Syverud K, Strand BL (2017). Mechanical Properties of Composite Hydrogels of Alginate and Cellulose Nanofibrils. Polymers-Basel, 9

Aarstad O, Strand BL, Klepp-Andersen LM, Skjak-Braek G (2013). Analysis of G-Block Distributions and Their Impact on Gel Properties of in Vitro Epimerized Mannuronan. Biomacromolecules, 14:3409-3416

Aarstad OA, Tondervik A, Sletta H, Skjak-Braek G (2012). Alginate Sequencing: An Analysis of Block Distribution in Alginates Using Specific Alginate Degrading Enzymes. Biomacromolecules, 13:106-116

Agoda-Tandjawa G, Durand S, Berot S, Blassel C, Gaillard C, Garnier C, Doublier JL (2010). Rheological characterization of microfibrillated cellulose suspensions after freezing. Carbohyd Polym, 80:677-686

583 Al-Hadithi TSR, Barnes HA, Walters K (1992). The Relationship between the Linear (Oscillatory) and
584 Nonlinear (Steady-State) Flow Properties of a Series of Polymer and Colloidal Systems.
585 Colloid Polym Sci, 270:40-46
586 Alexandrescu L, Syverud K, Gatti A, Chinga-Carrasco G (2013). Cytotoxicity tests of cellulose
587 nanofibril-based structures. Cellulose, 20:1765-1775 doi:DOI 10.1007/s10570-013-9948-9
588 Chinga-Carrasco G (2018). Potential and Limitations of Nanocelluloses as Components in
589 Biocomposite Inks for Three-Dimensional Bioprinting and for Biomedical Devices.
590 Biomacromolecules, 19:701-711
591 Chinga-Carrasco G, Averianova N, Kondalenko O, Garaeva M, Petrov V, Leinsvang B, Karlsen T (2014).
592 The effect of residual fibres on the micro-topography of cellulose nanopaper. Micron, 56:80-
593 84
594 Cox WP, Merz EH (1958). Correlation of Dynamic and Steady Flow Viscosities. J Polym Sci, 28:619-
595 622
596 Dai L et al. (2019). 3D printing using plant-derived cellulose and its derivatives: A review. Carbohyd
597 Polym, 203:71-86
598 De France KJ, Hoare T, Cranston ED (2017). Review of Hydrogels and Aerogels Containing
599 Nanocellulose. Chem Mater, 29:4609-4631
600 Donati I, Holtan S, Morch YA, Borgogna M, Dentini M, Skjak-Braek G (2005). New hypothesis on the
601 role of alternating sequences in calcium-alginate gels. Biomacromolecules, 6:1031-1040
602 Dong H, Snyder JF, Williams KS, Andzelm JW (2013). Cation-induced hydrogels of cellulose nanofibrils
603 with tunable moduli. Biomacromolecules, 14:3338-3345 doi:10.1021/bm400993f
604 Engler AJ, Sen S, Sweeney HL, Discher DE (2006). Matrix elasticity directs stem cell lineage
605 specification. Cell, 126:677-689
606 Habibi Y, Lucia LA, Rojas OJ (2010). Cellulose Nanocrystals: Chemistry, Self-Assembly, and
607 Applications. Chem Rev, 110:3479-3500 doi:Doi 10.1021/Cr900339w
608 Haug A, Larsen B, Smidsrod O (1967). Studies on Sequence of Uronic Acid Residues in Alginic Acid.
609 Acta Chem Scand, 21:691-&
610 Heggset EB, Chinga-Carrasco G, Syverud K (2017). Temperature stability of nanocellulose dispersions.
611 Carbohyd Polym, 157:114-121 doi:http://dx.doi.org/10.1016/j.carbpol.2016.09.077
612 Huan S, Ajdary R, Bai L, Klar V, Rojas OJ (2018). Low solids emulsion gels based on nanocellulose for
613 3D-printing. Biomacromolecules doi:10.1021/acs.biomac.8b01224
614 Leppiniemi J et al. (2017). 3D-Printable Bioactivated Nanocellulose-Alginate Hydrogels. Acs Appl
615 Mater Inter, 9:21959-21970
616 Lowys MP, Desbrieres J, Rinaudo M (2001). Rheological characterization of cellulosic microfibril
617 suspensions. Role of polymeric additives. Food Hydrocolloid, 15:25-32
618 Markstedt K, Mantas A, Tournier I, Martinez Ávila H, Hägg D, Gatenholm P (2015). 3D Bioprinting
619 Human Chondrocytes with Nanocellulose-Alginate Bioink for Cartilage Tissue Engineering
620 Applications. Biomacromolecules, 16:1489-1496 doi:10.1021/acs.biomac.5b00188
621 Martínez Ávila H, Schwarz S, Rotter N, Gatenholm P (2016). 3D bioprinting of human chondrocyte-
622 laden nanocellulose hydrogels for patient-specific auricular cartilage regeneration.
623 Bioprinting, 1-2:22-35 doi:https://doi.org/10.1016/j.bprint.2016.08.003
624 Muller M, Ozturk E, Arlov O, Gatenholm P, Zenobi-Wong M (2017). Alginate Sulfate-Nanocellulose
625 Bioinks for Cartilage Bioprinting Applications. Ann Biomed Eng, 45:210-223
626 Mørch YA, Donati I, Strand BL, Skjak-Braek G (2007). Molecular engineering as an approach to design
627 new functional properties of alginate. Biomacromolecules, 8:2809-2814
628 Mørch YA, Holtan S, Donati I, Strand BL, Skjåk-Bræk G (2008). Mechanical properties of C-5
629 epimerized alginates. Biomacromolecules, 9:2360-2368
630 Naderi A, Lindstrom T, Sundstrom J (2014). Carboxymethylated nanofibrillated cellulose: rheological
631 studies. Cellulose, 21:1561-1571
632 Nascimento DM et al. (2018). Nanocellulose nanocomposite hydrogels: technological and
633 environmental issues. Green Chem, 20:2428-2448

634 Peppas NA, Khare AR (1993). Preparation, Structure and Diffusional Behavior of Hydrogels in
635 Controlled-Release. Adv Drug Deliver Rev, 11:1-35
636 Piras CC, Fernandez-Prieto S, De Borggraeve WM (2017). Nanocellulosic materials as bioinks for 3D
637 bioprinting. Biomater Sci-Uk, 5:1988-1992
638 Poonguzhali R, Basha SK, Kumari VS (2017). Synthesis and characterization of chitosan-PVP-
639 nanocellulose composites for in-vitro wound dressing application. International Journal of
640 Biological Macromolecules, 105:111-120
641 Pääkkö M et al. (2007). Enzymatic hydrolysis combined with mechanical shearing and high-pressure
642 homogenization for nanoscale cellulose fibrils and strong gels. Biomacromolecules, 8:1934-
643 1941 doi:Doi 10.1021/Bm061215p
644 Rashad A et al. (2018). Coating 3D Printed Polycaprolactone Scaffolds with Nanocellulose Promotes
645 Growth and Differentiation of Mesenchymal Stem Cells. Biomacromolecules
646 doi:10.1021/acs.biomac.8b01194
647 Rashad A, Mustafa K, Heggset EB, Syverud K (2017). Cytocompatibility of Wood-Derived Cellulose
648 Nanofibril Hydrogels with Different Surface Chemistry. Biomacromolecules, 18:1238-1248
649 Rees A, Powell LC, Chinga-Carrasco G, Gethin DT, Syverud K, Hill KE, Thomas DW (2015). 3D
650 Bioprinting of Carboxymethylated-Periodate Oxidized Nanocellulose Constructs for Wound
651 Dressing Applications. Biomed Res Int
652 Saito T, Isogai A (2004). TEMPO-mediated oxidation of native cellulose. The effect of oxidation
653 conditions on chemical and crystal structures of the water-insoluble fractions.
654 Biomacromolecules, 5:1983-1989
655 Saito T, Isogai A (2006). Introduction of aldehyde groups on surfaces of native cellulose fibers by
656 TEMPO-mediated oxidation. Colloid Surface A, 289:219-225 doi:DOI
657 10.1016/j.colsurfa.2006.04.038
658 Siqueira G et al. (2017). Cellulose Nanocrystal Inks for 3D Printing of Textured Cellular Architectures.
659 Adv Funct Mater, 27
660 Smidsrod O (1972). Properties of Poly(1,4-Hexuronates) in Gel State .2. Comparison of Gels of
661 Different Chemical Composition. Acta Chem Scand, 26:79-88
662 Sultan S, Siqueira G, Zimmermann T, Mathew AP (2017). 3D printing of nano-cellulosic biomaterials
663 for medical applications. Current Opinion in Biomedical Engineering, 2:29-34
664 Syverud K (2017) Tissue engineering using plant derived cellulose nanofibrils (CNF) as scaffold
665 material. In: Atalla R, Isogai A, Agarwal U (eds) Nanocelluloses, their Preparation, Properties,
666 and Applications. ACS books,
667 Unnithan AR, Sasikala ARK, Sathishkumar Y, Lee YS, Park CH, Kim CS (2014). Nanoceria doped
668 electrospun antibacterial composite mats for potential biomedical applications. Ceram Int,
669 40:12003-12012
670 Wang QQ, Sun JZ, Yao Q, Ji CC, Liu J, Zhu QQ (2018). 3D printing with cellulose materials. Cellulose,
671 25:4275-4301
672 Wågberg L, Decher G, Norgren M, Lindström T, Ankerfors M, Axnäs K (2008). The build-up of
673 polyelectrolyte multilayers of microfibrillated cellulose and cationic polyelectrolytes.
674 Langmuir, 24:784-795 doi:Doi 10.1021/La702481v
675 Xu WY, Wang XJ, Sandler N, Willfor S, Xu CL (2018). Three-Dimensional Printing of Wood-Derived
676 Biopolymers: A Review Focused on Biomedical Applications. Acs Sustain Chem Eng, 6:5663-
677 5680
678 Zander NE, Dong H, Steele J, Grant JT (2014). Metal Cation Cross-Linked Nanocellulose Hydrogels as
679 Tissue Engineering Substrates. Acs Appl Mater Inter, 6:18502-18510

680

681

682

Graphical abstract